JOURNAL OF SOLID STATE CHEMISTRY 117, 373–378 (1995)

A Comparative Study of a Novel Microporous Indiumphosphate and Other M(III)X(V)O_4-Type Microporous Materials

Y. Xu[1]

Division of Chemistry, School of Science/NIE, Nanyang Technological University, 469 Bukit Timah Road, Singapore 1025

L. L. Koh and L. H. An

Department of Chemistry, National University of Singapore, Kent Ridge 0511, Singapore

and

R. R. Xu and S. L. Qiu

Key Laboratory of Inorganic Hydrothermal Synthesis, Jilin University, Changchun 130023, People's Republic of China

Received June 6, 1994; in revised form November 21, 1994; accepted November 28, 1994

A novel microporous indiumphosphate, $InPO_4(H_2O)_2 \cdot 0.1Et_3N$ ($InPO_4$-1) is synthesized from the hydrothermal reaction of H_3PO_4, In_2O_3, and H_2O in the presence of triethylamine, or *n*-butylamine, dimethylamine, dipropylamine, ethylenediamine, and tetramethylammonium hydroxide. Single crystal X-ray diffraction studies show that $InPO_4$-1 has orthorhombic symmetry, space group *Pbca*, with a = 8.842(2) Å, b = 10.1870(10) Å, c = 10.327(2) Å, V = 930.1(3) Å^3, and Z = 8. It has a three-dimensional microporous structure with one-dimensional 6- and 4-rings running along the *b*- and *a*-axes, respectively. In and P occupy framework positions forming [$InO_4(H_2O)_2$] octahedral and [PO_4] tetrahedral geometry, and they alternate through O bridges. $InPO_4$-1 has poor thermal stability and its microporous structure is comparable to small-pore $AlPO_4$-*n*. Organic amines that are used in the preparation of $InPO_4$-1 range from primary amine to quaternary ammonia although the mechanism has yet to be understood. © 1995 Academic Press, Inc.

1. INTRODUCTION

Recent advances in microporous crystalline materials are represented by the discovery of $AlPO_4$-*n* (1, 2), M(III)X(V)O_4-type materials including $GaPO_4$-*n* (3–5), $AlAsO_4$-*n*, $GaAsO_4$-*n* (6–8), GeO_2 series (9), and inclusion compounds with aluminophosphate composition (10). Some of these compounds are structural analogues of zeolites, but the majority possess novel structural types with 3D, 2D, and 1D framework structures. The development of the chemistry of microporous materials has been following the "Periodic Table Strategy" as is evident in recent work (11). The strategy of synthesis of microporous materials has been strongly associated with the choice of organic base and solvent (12), steric and electronic considerations, and the coordination habit of elements (11, 12). Among M(III)X(V)O_4-type microporous materials, the structural variety, channel dimension, and thermal stability decrease in the order $AlPO_4$-*n* > $GaPO_4$-*n* > $AlAsO_4$-*n* > $GaAsO_4$-*n* (11, 12). In the present paper, we report the synthesis and characterization of a novel microporous indiumphosphate, $InPO_4$-1, the first microporous indiumphosphate ($InPO_4$-*n*). The similarity and difference between $InPO_4$-1 and M(III)X(V)O_4-type materials are discussed.

2. EXPERIMENTAL

$InPO_4$-1 was prepared hydrothermally from a typical batch composition of $1.0In_2O_3 : 1.2P_2O_5 : (1.0 \sim 2.0)$ Et_3N (or, *n*-BuA, DMA, DPA, EDA, and TMAOH) : (80–180)H_2O at pH between 3.0 ~ 6.0. Crystallization was conducted at 180°C for 7 to 15 days under autogeneous pressure. Pale-greenish microcrystallites were recovered by filtering, washing with distilled water, and drying at ambient temperature overnight.

A single crystal X-ray diffraction study was made on a selected crystal of dimensions 0.15 × 0.15 × 0.20 mm. Unit cell parameters were determined by least-squares fits to the setting parameters of 20 centered reflections. Intensities of 820 independent reflections (3.5° < 2θ < 50°) were measured by ω scan on a Siemens R3M/V2000 diffractometer with Mo$K\alpha$ radiation. Lorentz and Polar-

[1] To whom correspondence should be addressed.

0022-4596/95 $12.00

TABLE 1
Details of the Single Crystal X-Ray Diffraction Experiment

Chemical formula	$InPO_4(H_2O)_2 \cdot 0.1Et_3N$
Wavelength (Mo$K\alpha$)	0.71073 Å
Temperature	25°C
Monochromator	Graphite
Absorption correction	Semiempirical (psi scan)
Transmission factors	0.763–0.790
Absorption coefficient	5.365 mm^{-1}
Scan type	ω
Number of reflections	820
Independent reflections (R_{int} = 0.00%)	820
Observed reflections ($F > 4.0\sigma(F)$)	772
Weighting scheme	$w^{-1} = \sigma^2(F) + 0.0007\, F^2$
Extinction correction	$\chi = 0.00078(8)$ $F^* = F[1 + 0.002\chi F^2/\sin(2\theta)]^{-1/4}$

ization corrections were applied. Absorption was corrected using the semiempirical method by psi-scan. The crystal structure was solved by direct methods, and refined by full-matrix least-squares analysis to final values of $R = 0.015$ and $wR = 0.024$. The function minimized was $\Sigma\, w(F_o - F_c)^2$. Nonhydrogen atoms were refined anisotropically. The positions of hydrogen atoms, located from difference map, were not refined. Experimental details are summarized in Table 1.

Bulk samples including as-synthesized and calcined precursors which were heated at different temperatures for 15 min were studied using XRD, FTIR, TG, ^{31}P MASNMR, SEM/EDAX, and chemical analysis. The XRD pattern was recorded at RT for 2θ (3.5° to 60°) on a Rigaku D/Max IIIA diffractometer (Cu$K\alpha$ radiation). Based on single crystal X-ray data assuming Cu$K\alpha$ radiation, a simulated XRD pattern was obtained. FTIR spectra were recorded on a Perkin–Elmer FTIR Model 1725x spectrometer in the range 4000 to 450 cm^{-1} in air. Thermalgravimetry analysis was carried out using a Du Point 9900 thermal analyzer from RT to 1000°C under N_2 atmosphere. ^{31}P MASNMR data were acquired on a Bruker MSL-400 NMR spectrometer resonating at 161.92 MHz using 85% H_3PO_4 as standard. Spinning speeds of typically 2.5–3 kHz were achieved. SEM/EDAX were conducted using a Hitachi 650B electron microscope for the as-synthesized precursor which was polished in a supersonic acetone bath. Adsorption measurements were carried out on calcined precursors using a CAHN-2000 model which was equipped with an *in situ* activation setup. In and P contents were analyzed using ICP and those of C, N, and H by elemental analysis.

In order to confirm Et_3N content, the as-synthesized precursor of $InPO_4$-1 was heated to 1000°C while gaseous outlet was collected using a graphitized carbon black cartridge and an octadecane-bonded silica cartridge. The outlet was washed out using methanol and analyzed using gas chromotography (HP 5890A GC) with a capillary column of dimensions 25 m × 0.32 mm. GC was equipped with FID and NPD detectors running simultaneously at 250 and 220°C, respectively. The injection temperature was 200°C, and the oven was programmed from 55°C (isotherm for 2 min) to 100°C at a heating rate of 8°C/min.

3. RESULTS AND DISCUSSION

3.1. Synthesis and Characterization of Microporous Indiumphosphate, $InPO_4$-1

Based on chemical analysis, the as-synthesized precursor of $InPO_4$-1 has a bulk composition of $H_4InPO_6 \cdot 0.1Et_3N$, but the actual content of Et_3N inside crystallites remains uncertain. The crystal structure of $InPO_4$-1 shows a novel feature as demonstrated by XRD patterns in Figs. 1a and 4. The experimental and the simulated XRD patterns match well at the position of reflections with only small differences in the relative intensity of some reflections (Fig. 1b). Hence, the product is monophasic. The difference in the relative intensity could be the consequence of many factors, for example, the presence of physisorbed H_2O and Et_3N as well as particle size and morphology causing a preferred orientation. The ^{31}P NMR spectrum of $InPO_4$-1 shows a single resonance peak at ~ −2.17 ppm which suggests that all P atoms in crystal structure are chemically equivalent. In and P distribute homogeneously over the bulk sample at a ratio of around 1 : 1 as demonstrated by SEM/EDAX analyses.

According to the single-crystal X-ray diffraction study, $InPO_4$-1 crystallizes in the orthorhombic symmetry of space group *Pbca*. One asymmetric unit consists of $InPO_4(H_2O)_2$ (Fig. 2a). There is one crystallographically

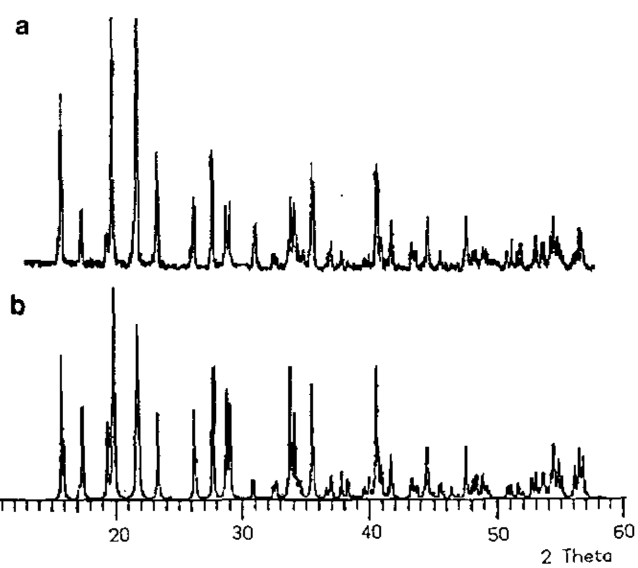

FIG. 1. The XRD patterns of the indiumphosphate: (a) experimental; (b) simulated based on the single crystal X-ray diffraction analysis.

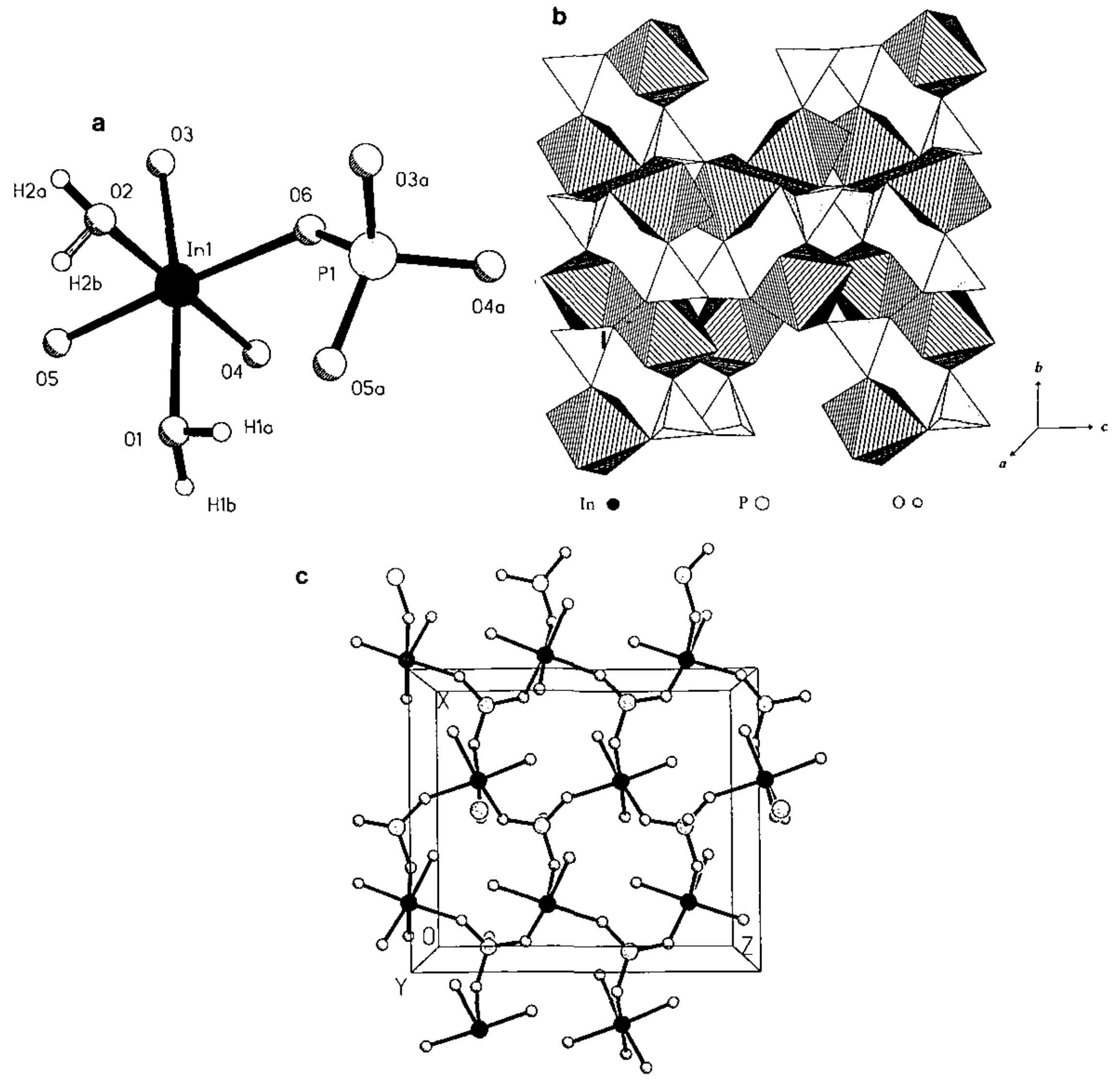

FIG. 2. (a) Atomic numbering; (b) packing view along the *a*-axis; (c) packing view along the *b*-axis.

independent site for the In and P atoms which is in agreement with the ^{31}P NMR study. In and P atoms alternate and are bridged through O atoms. P atoms are tetrahedrally coordinated to 4 O atoms with P–O contact varying between 1.531(4) and 1.546(1) Å and O–P–O angles varying between 107.8(2)° and 111.1(1)° (see Tables 2, 3a, and 3b). This P–O bond length is greater than that in $AlPO_4$-*n* (~1.52 Å) and $GaPO_4$-*n* (~1.526 Å); however, it is a little shorter than the P–O bond in H_3PO_4 (1.57 Å) (13). The ^{31}P NMR signal shifts to high-field direction as the P–O contact increases, for example, −28 ppm for $AlPO_4$-*n*, −11 to −25 ppm for $GaPO_4$-*n*, and −2.17 ppm for $InPO_4$-1. This is in good agreement with previous findings (14, 15). In atoms have six-coordination with O ligands where four are bridging oxygen atoms with an In–O bond length varying between 2.106(1) and 2.131(1) Å, and the remaining two bond to H forming structural H_2O

TABLE 2
Atomic Coordinates ($\times 10^4$) for $[InPO_4(H_2O)_2]$

Atom	*x*	*y*	*z*
In(1)	1527(1)	6723(1)	8691(1)
P(1)	327(4)	3581(1)	8481(1)
O(1)	3440(1)	5560(1)	9484(1)
O(2)	2332(1)	6048(1)	6840(1)
O(3)	−62(1)	8040(1)	7887(1)
O(4)	816(1)	7086(1)	10604(1)
O(5)	3045(1)	8324(1)	8919(1)
O(6)	49(1)	5079(1)	8520(1)
H(1a)	3192	4748	9443
H(1b)	3726	5733	10298
H(2a)	2241	6601	6328
H(2b)	3282	5805	6770

TABLE 3a
Selected Bond Lengths

Bond	Bond length (Å)
In(1)-O(1)	2.222(1)
In(1)-O(2)	2.152(1)
In(1)-O(3)	2.112(1)
In(1)-O(4)	2.106(1)
In(1)-O(5)	2.126(1)
In(1)-O(6)	2.132(1)
P(1)-O(6)	1.546(1)
P(1)-O(3a)	1.535(1)
P(1)-O(4a)	1.541(3)
P(1)-O(5a)	1.531(4)

molecules (In1–O1 and In1–O2 being 2.152(1) and 2.222(1) Å, respectively). Hence, the primary building unit of In is composed of $[InO_4(H_2O)_2]$, where the O–In–O bond angle falls in the range of 83.0(1)° to 97.7(1)°. The $[InO_4(H_2O)_2]$ unit has distorted octahedral geometry which is attributed to the different coordination strengths of O^{2-} and H_2O ligands. In comparison with the average P–O bond length in $AlPO_4$-*n* (1.52 Å), the P–O bond in $InPO_4$-1 is much greater (1.538 Å), suggesting that the bond strength of In–O is stronger than that of Al–O, thus weakening P–O bonding.

The 6- and 4-rings of $InPO_4$-1 form one-dimensional channels along the *b*- and *a*-axes, respectively (Figs. 2b and 2c). There are also "8"-ring openings along the *a*-axis, each of which is surrounded by four 4-rings. However, six out of the eight T-atoms of the 8-ring are shared with the

TABLE 3b
Selected Bond Angles

Bond	Bond angles (°)
O(1)-In(1)-O(2)	84.6(1)
O(1)-In(1)-O(3)	171.8(1)
O(2)-In(1)-O(3)	94.2(1)
O(1)-In(1)-O(4)	88.6(1)
O(2)-In(1)-O(4)	171.1(1)
O(3)-In(1)-O(4)	93.4(1)
O(1)-In(1)-O(5)	83.5(1)
O(2)-In(1)-O(5)	97.7(1)
O(3)-In(1)-O(5)	88.6(1)
O(4)-In(1)-O(5)	87.1(1)
O(1)-In(1)-O(6)	94.5(1)
O(2)-In(1)-O(6)	83.0(1)
O(3)-In(1)-(6)	93.4(1)
O(4)-In(1)-O(6)	91.9(1)
O(5)-In(1)-O(6)	177.8(1)
O(6)-P(1)-O(3a)	110.7(1)
O(6)-P(1)-P(4a)	108.4(2)
O(3a)-P(1)-O(4a)	107.8(2)
O(6)-P(1)-O(5a)	108.1(2)
O(3a)-P(1)-O(5a)	110.7(2)
O(4a)-P(1)-O(5a)	111.1(1)

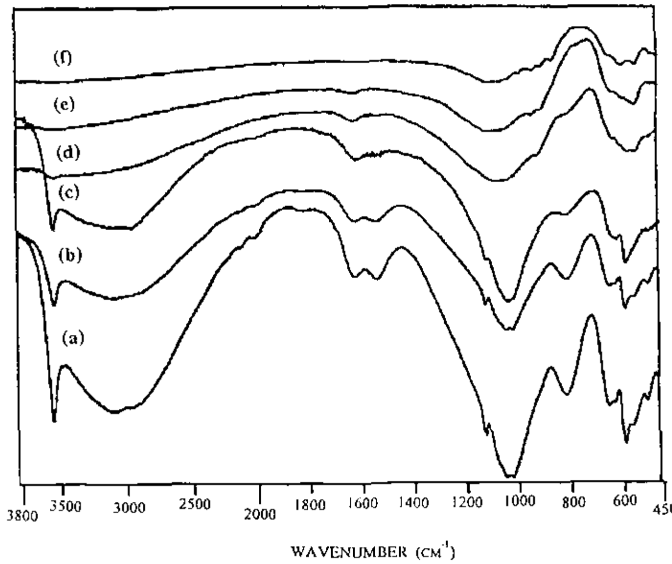

FIG. 3. *In situ* FTIR results of the indiumphosphate recorded in air.

6-ring channel nearly perpendicular to it. This results in a cage-like building unit which consists of 6- and 8-rings. Lying on the *ac* plane are a net of 6-rings which join up via either an $[InO_4(H_2O)_2]$ octahedron or a PO_4 tetrahedron by sharing corners (Fig. 2c). The $[InO_4(H_2O)_2]$ unit of one layer has a H_2O molecule stretching to the 6-ring window, and the $[InO_4(H_2O)_2]$ unit of the next layer has the H_2O molecule pointing to it from a different direction. Hence, the effective diameter of the 6-ring channel is significantly reduced. Structural H_2O molecules can be classified into two types, H-bonded (OH $\cdots$ O $\approx$ 2.6 Å) and non-H-bonded (OH $\cdots$ O′ $\geq$ 3 Å). This is supported by the sharp and narrow IR adsorption at 3535 cm^{-1} and the hump between 3400 and 2800 cm^{-1} (Fig. 3). Et_3N and adsorbed H_2O molecules are hardly detected, not even from the set of X-ray crystallographic data collected at −60°C. However, these "guest" species do exist as indicated by the rejected reflections which violate the *Pbca* symmetry of $InPO_4$-1. By analyzing the fragments driven from the as-synthesized precursor using GC, a trace amount of Et_4N is detected. It is clear that there is a small amount of "guest" species distributed in the pore spacing of the crystal structure, or possibly adsorbed on the crystallite surfaces of $InPO_4$-1.

In situ FTIR results are shown in Fig. 3. The absorption band at 3535 cm^{-1} is attributed to O–H of the structural H_2O molecules. The hump between 3400 and 2800 cm^{-1} can be significantly weakened if the spectrum is acquired under an N_2 atmosphere. It possibly indicates the weak H_2O $\cdots$ H bonds among the structural H_2O molecules and between the structural and physisorbed H_2O molecules. As the as-synthesized precursor is heated to above 300°C, the intensity of 3535 cm^{-1} absorption declines dras-

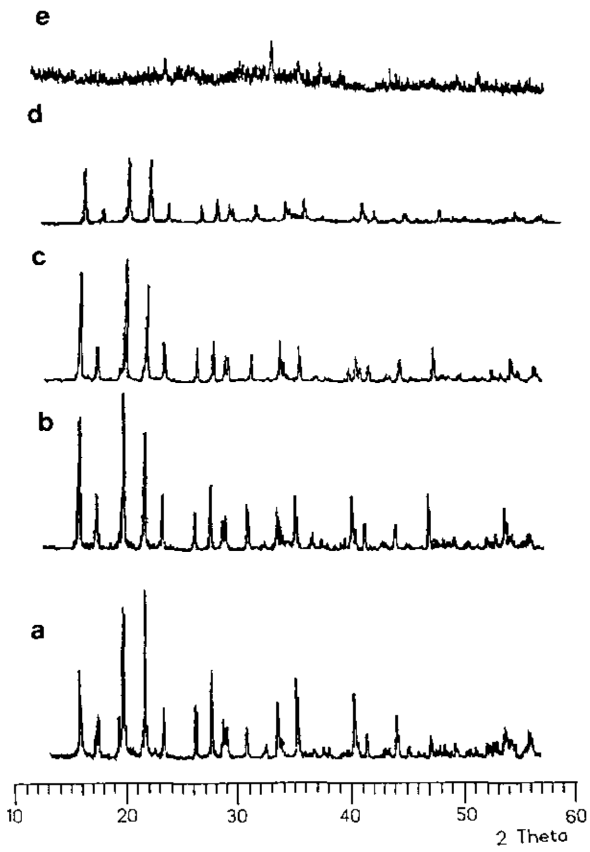

FIG. 4. *In situ* XRD results of the indiumphosphate.

tically, and so does the hump between 3400 and 2800 cm^{-1}. This is due to the removal of the structural H_2O molecules. The absorptions between 700 and 500 cm^{-1}, which characterize 6- and 4-rings, start to deform at temperatures above 300°C. As shown by *in situ* XRD studies (Fig. 4), $InPO_4$-1 gradually loses crystallinity below 300°C

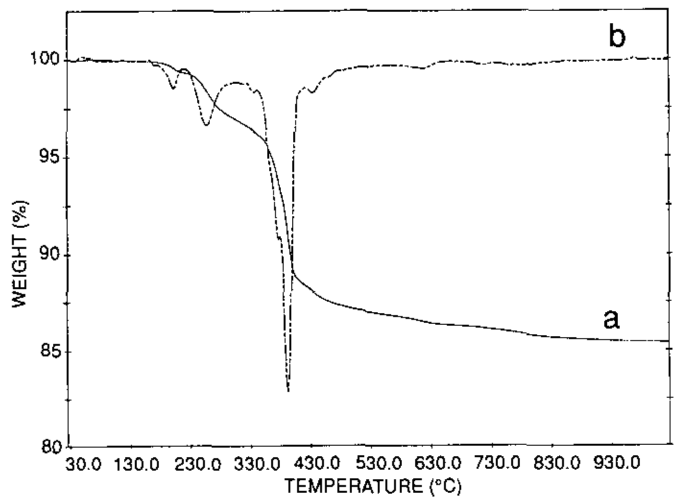

FIG. 5. The TG results of the indiumphosphate: (a) TG curve; (b) the first derivative curve of the TG result.

whereas its crystal structure remains intact. Hence, significant structural transformation does not occur until the calcination temperature reaches 400°C.

TG analysis indicates that there are four major changes at 130–180°C, 180–300°C, 300–610°C, and 610–950°C with weight losses of about 0.76, 2.97, 10.31, and 1.25%, respectively (Fig. 5). They are associated with following processes:

- removal of physisorbed H_2O;
- partial dehydration of the structural H_2O molecules and detemplation causing a minor loss of crystallinity;
- dehydration between the structural H_2O molecules causing a drastic degradation of the crystal structure (Fig. 4);
- complete collapse of the crystal structure.

3.2. Comparative Study of Microporous Indiumphosphate and Other M(III)X(V)O_4-Type Materials

Coordination habit. As previously discussed, In atoms in $InPO_4$-1 have six-coordination forming $[InO_4(H_2O)_2]$. Two "extra" H_2O ligands give slightly longer In–O_{ex} contact (average, 2.187 Å) than that of the bridging O_f (average, 2.119 Å). The O_{ex}–In–O_{ex} angle (average, 84.6°) is smaller than that of O_f–In–O_f (average, 90.5°). This may relate to the strong negative charge of O_{ex} which makes H_2O_{ex} a stronger ligand than O_f. M^{3+} having coordination number greater than four has been found in some M(III)X(V)O_4-type compounds. For example, $AlPO_4$-12, -17, and -EN3 contain five-coordinated Al^{3+} (17); $AlPO_4$-14 contains both five- and six-coordinated Al^{3+} and $AlPO_4$-15 has six-coordinated Al^{3+} (18) where "extra" ligands are solely terminal OH^- groups. In $GaPO_4$-n, Ga^{3+} has exclusively five- or six-coordinate geometry. "Extra" ligands are often OH^- groups [e.g., $GaPO_4$-C3 (19) and $GaPO_4$-14 (20)], and occasionally H_2O molecules [e.g., $GaPO_4$-C7 (21) and $GaPO_4$-C14 (22)], or F^- ion [e.g., cloverite (23)]. Similar phenomena are observed in $AlAsO_4$-n ($AlAsO_4$-1 and $AlAsO_4$-2) (12) and $GaAsO_4$-n ($GaAsO_4$-2) (12). Obviously, as the ionic radius of M^{3+} increases, a more "crowded" coordination environment is preferred, and the M^{3+} seems to affiliate more strongly to H_2O than to the OH^- group. The former phenomena could be a result of the underlying d^{10} configuration of Ga^{3+} and In^{3+} which takes part in $d\pi$–$d\pi$ back bonding. The latter is more related to the decreasing charge/radius ratio of M^{3+} which weakens its hardness as an electron acceptor. As a result, the Brønsted basicity of O_{ex} increases, and a structural H_2O ligand is preferred over OH^-. It is likely that the moderate to weak acidic medium of synthesis (pH 3.0 ~ 6.0) provides a good source of H^+ for OH^- to be neutralized.

Structural characteristics. $InPO_4$-1 crystallizes in orthorhombic symmetry with one-dimensional 4- and 6-ring channels parallel to the *a*- and *b*-axes, respectively. The window of the 6-ring channel is partially blocked by the structural H_2O molecules, hence, the effective diameter is much smaller than that of an ordinary 6-T ring. This explains why $InPO_4$-1 exhibits little adsorptive capacity. $InPO_4$-1 is comparable to small pore $AlPO_4$-*n*. As a comparison, most $GaPO_4$-*n* have a pore dimension equivalent to or smaller than that of a 10-ring (except for cloverite). Upon the removal of template species, they show typical reversible adsorption–desorption features of microporous materials. The micropore of $AlPO_4$-*n* ranges from an 8- to a 20-ring. They are able to adsorb molecules of various sizes. It appears that as the ionic radius of M^{3+} increases, the tendency to form M(III)P(V)O_4-type microporous compounds decreases. Consistent with this observation, M(III)P(V)O_4-type materials show decreasing thermal stability in the order $AlPO_4$-*n* > $GaPO_4$-*n* > $InPO_4$-1. Similar phenomena have also been observed among M(III) As(V)O_4 compounds (M = Al^{3+} and Ga^{3+}) (12). This is clearly associated with an increasing $r_{M/X}$ ratio.

The role of organic species. As shown in present study, Et_3N is not the only organic amine available for hydrothermal synthesis of $InPO_4$-1. *n*-BuA, DMA, DPA, EDA, or TMAOH can play the same role during the crystallization of $InPO_4$-1. These amines have drastically different configurations and properties whereas they appear consistently in a small amount in the as-synthesized precursor, such as $InPO_4(H_2O)_2 \cdot 0.1Et_3N$. Previous studies demonstrate that large pore structures tend to be less critical to the size and shape of organic templates. Among known M(III)P(V)O_4-type materials, the decreasing capacity to occlude organic amines has been found, $AlPO_4$-*n* > $GaPO_4$-*n* > $AlAsO_4$-*n* > $GaAsO_4$-*n* (12). In comparison, $InPO_4$-1 shows the least ability to occlude organic amines. This gives an updated order $AlPO_4$-*n* > $GaPO_4$-*n* > $AlAsO_4$-*n* > $GaAsO_4$-*n* > $InPO_4$-1. Again, the greater $r_{In(III)/P(V)}$ ratio and the distorted tetrahedral geometry of InO_4 are believed to be the main factors.

4. CONCLUSION

Microporous indiumphosphate $InPO_4$-1 is composed of an $InPO_4(H_2O)_2$ framework where In^{3+} has octahedral geometry and P^{5+} has tetrahedral geometry. The crystal structure contains 4- and 6-ring one-dimensional channels. The 6-ring channels are partially blocked by the structural H_2O molecules which reduce the effective diameter significantly. $InPO_4$-1 shows typical features of microporous structures; however, it exhibits essentially no adsorptive properties. In comparison with other M(III)P(V)O_4-type materials, the microporous structure of $InPO_4$ is more difficult to construct, and is more vulnerable to thermal treatment. This is believed to be the result of the small charge/radius ratio of In^{3+} and the large $r_{In(III)/P(V)}$ ratio of indiumphosphate.

ACKNOWLEDGMENTS

We thank our colleagues Mr. Hai-Bin Wan of the Department of Chemistry, National University of Singapore and Professors Yi-Hua Xu and Yong Yue of the Key Laboratory of Inorganic Hydrothermal Synthesis, Jilin University, People's Republic of China, for their technique assistance and valuable advice. We also acknowledge the National University of Singapore for financial support.

REFERENCES

1. S. T. Wilson, B. M. Lok, C. A. Messina, T. R. Cannon, and E. M. Flanigen, *ACS Symp. Ser.* **218,** 799 (1983).
2. S. T. Wilson, B. M. Lok, C. A. Messina, T. R. Cannon, and E. M. Flanigen, *J. Am. Chem. Soc.* **104,** 1146 (1982).
3. J. B. Parise, *J. Chem. Soc. Chem. Commun.,* 606 (1985).
4. S. H. Feng, Ph.D. Thesis, Jilin University, 1986.
5. S. H. Feng and R. R. Xu, *Chem. J. Chinese Univ.* (*Chin. Ed.*), **8,** 867 (1987).
6. J. S. Chen and R. R. Xu, *J. Solid State Chem.* **80,** 149 (1989).
7. G. D. Yang, L. Li, J. S. Chen, and R. R. Xu, *J. Chem. Soc. Chem. Commun.,* 810 (1989).
8. J. S. Chen, L. Li, G. D. Yang, and R. R. Xu, *J. Chem. Soc. Chem. Commun.,* 1217 (1989).
9. S. G. Li, R. R. Xu, Y. Q. Lu and Y. H. Xu, *in* "Proceedings 9th International Zeolite Conference, Montreal" (R. von Ballmoos, J. B. Higgins, and M. M. J. Treacy, Eds.), p. 345. Butterworth–Heinemann, Guildford, UK, 1992.
10. R. R. Xu, Q. S. Huo, and W. Q. Pang, *in* "Proceedings, 9th International Zeolite Conference, Montreal" (R. von. Ballmoos, J. B. Higgins, and M. M. J. Treacy, Eds.), p. 271. Butterworth–Heinemann, 1992.
11. E. M. Flanigen, B. M. Lok, T. R. Patton, and S. T. Wilson, *in* "Proceedings, 7th. International Zeolite Conference, Tokyo" (Y. Murakami, A. Lijima, and J. W. Ward, Eds.), p. 103. Kodansha/Elsevier, Tokyo/Amsterdam, 1986.
12. R. R. Xu, J. S. Chen, and S. H. Feng, *in* "Chemistry of Microporous Crystals" (T. Inui, S. Namba, and T. Tatsumi, Eds.), p. 63. Kodansha/Elsevier, Tokyo/Amsterdam, 1990.
13. N. N. Greenwood and A. Earnshaw, "Chemistry of the Elements," p. 595. Pergamon Press, Oxford, 1984.
14. A. K. Cheetham, N. J. Clayden, C. M. Dobson, and R. J. B. Jakeman, *J. Chem. Soc. Chem. Commun.,* 195 (1986).
15. D. G. Govenstein, "Phosphorus-31 NMR, Principles and Applications." Academic Press, New York, 1984.
16. J. V. Smith, *Chem. Rev.* **88,** 149 (1988).
17. J. M. Bennett, W. J. Dytrych, J. J. Pluth, J. W. Richardson, and J. V. Smith, *Zeolites* **6,** 349 (1986).
18. J. V. Smith, *Chem. Rev.* **88,** 149 (1988).
19. G. D. Yang, S. H. Feng, and R. R. Xu, *J. Chem. Soc. Chem. Commun.,* 1254 (1987).
20. S. H. Feng and R. R. Xu, *Chem. J. Chinese Univ.* (*Engl. Ed.*) **2,** 1 (1988).
21. T. Wang, G. D. Yang, S. H. Feng, and R. R. Xu, *J. Chem. Soc. Chem. Commun.,* 945 (1989).
22. J. B. Parise, *J. Chem. Soc. Chem. Commun.,* 606 (1985).
23. M. Estermann, L. B. McCuster, C. Baerlocher, A. Merrouche, and H. Kessler, *Nature* **352,** 320 (1991).